Icarus 315 (2018) 146–157

Contents lists available at ScienceDirect

Icarus

journal homepage: www.elsevier.com/locate/icarus

Loss of the Martian atmosphere to space: Present-day loss rates determined from *MAVEN* observations and integrated loss through time

B.M. Jakosky[a,*], D. Brain[a], M. Chaffin[a], S. Curry[l], J. Deighan[a], J. Grebowsky[f], J. Halekas[r], F. Leblanc[i], R. Lillis[l], J.G. Luhmann[l], L. Andersson[a], N. Andre[b], D. Andrews[c], D. Baird[d], D. Baker[a], J. Bell[e], M. Benna[f], D. Bhattacharyya[g], S. Bougher[a,h], C. Bowers[a], P. Chamberlin[a], J.-Y. Chaufray[i], J. Clarke[g], G. Collinson[f], M. Combi[h], J. Connerney[f], K. Connour[a], J. Correira[j], K. Crabb[a], F. Crary[a], T. Cravens[k], M. Crismani[a], G. Delory[l], R. Dewey[a], G. DiBraccio[f], C. Dong[m], Y. Dong[a], P. Dunn[l], H. Egan[a], M. Elrod[f], S. England[n], F. Eparvier[a], R. Ergun[a], A. Eriksson[c], T. Esman[o], J. Espley[f], S. Evans[j], K. Fallows[g], X. Fang[a], M. Fillingim[l], C. Flynn[g], A. Fogle[l], C. Fowler[a], J. Fox[p], M. Fujimoto[q], P. Garnier[b], Z. Girazian[f], H. Groeller[o], J. Gruesbeck[f], O. Hamil[k], K.G. Hanley[a], T. Hara[l], Y. Harada[r], J. Hermann[a], M. Holmberg[b], G. Holsclaw[a], S. Houston[k], S. Inui[s], S. Jain[a], R. Jolitz[a], A. Kotova[b], T. Kuroda[t], D. Larson[l], Y. Lee[l], C. Lee[f], F. Lefevre[i], C. Lentz[a], D. Lo[o], R. Lugo[u], Y.-J. Ma[v], P. Mahaffy[f], M.L. Marquette[l], Y. Matsumoto[s], M. Mayyasi[g], C. Mazelle[b], W. McClintock[a], J. McFadden[l], A. Medvedev[w], M. Mendillo[g], K. Meziane[C], Z. Milby[a], D. Mitchell[l], R. Modolo[i], F. Montmessin[i], A. Nagy[h], H. Nakagawa[t], C. Narvaez[g], K. Olsen[h], D. Pawlowski[x], W. Peterson[a], A. Rahmati[l], K. Roeten[h], N. Romanelli[i], S. Ruhunusiri[r], C. Russell[v], S. Sakai[s], N. Schneider[a], K. Seki[s], R. Sharrar[h], S. Shaver[a], D.E. Siskind[y], M. Slipski[a], Y. Soobiah[f], M. Steckiewicz[b], M.H. Stevens[y], I. Stewart[a], A. Stiepen[z], S. Stone[o], V. Tenishev[h], N. Terada[t], K. Terada[t], E. Thiemann[a], R. Tolson[e], G. Toth[h], J. Trovato[g], M. Vogt[g], T. Weber[a], P. Withers[g], S. Xu[l], R. Yelle[o], E. Yiğit[A], R. Zurek[B]

[*] Corresponding author.

E-mail addresses: Bruce.jakosky@lasp.colorado.edu (B.M. Jakosky), david.brain@lasp.colorado.edu (D. Brain), michael.chaffin@coloradol.edu (M. Chaffin), smcurry@ssl.berkeley.edu (S. Curry), justin.deighan@lasp.colorado.edu (J. Deighan), joseph.m.grebowsky@nasa.gov (J. Grebowsky), jasper-halekas@uiowa.edu (J. Halekas), francois.leblanc@latmos.ipsl.fr (F. Leblanc), rlillis@ssl.berkeley.edu (R. Lillis), jgluhman@ssl.berkeley.edu (J.G. Luhmann), laila.andersson@lasp.colorado.edu (L. Andersson), nicolas.andre@irap.omp.eu (N. Andre), david.andrews@irfu.se (D. Andrews), darren.t.baird@nasa.gov (D. Baird), daniel.baker@lasp.colorado.edu (D. Baker), mehdi.benna-1@nasa.gov (M. Benna), dolonb@bu.edu (D. Bhattacharyya), bougher@umich.edu (S. Bougher), charlie.bowers@lasp.colorado.edu (C. Bowers), phil.chamberlin@lasp.colorado.edu (P. Chamberlin), chaufray@latmos.ipsl.fr (J.-Y. Chaufray), jclarke@bu.edu (J. Clarke), glyn.a.collinson@nasa.gov (G. Collinson), mcombi@umich.edu (M. Combi), jack.connerney@nasa.gov (J. Connerney), kyle.connour@colorado.edu (K. Connour), correira@cpi.com (J. Correira), kyle.crabb@lasp.colorado.edu (K. Crabb), frank.crary@lasp.colorado.edu (F. Crary), cravens@ku.edu (T. Cravens), matteo.crismani@colorado.edu (M. Crismani), gdelory@berkeley.edu (G. Delory), ryan.dewey@colorado.edu (R. Dewey), gina.a.dibraccio@nasa.gov (G. DiBraccio), dcfy@princeton.edu (C. Dong), yaxue.dong@lasp.colorado.edu (Y. Dong), pdunn@ssl.berkeley.edu (P. Dunn), hilary.egan@colorado.edu (H. Egan), meredith.k.elrod@nasa.gov (M. Elrod), england@ssl.berkeley.edu (S. England), eparvier@colorado.edu (F. Eparvier), bob.ergun@lasp.colorado.edu (R. Ergun), anders.eriksson@irfu.se (A. Eriksson), tesman@lpl.arizona.edu (T. Esman), jared.espley@nasa.gov (J. Espley), evans@cpi.com (S. Evans), kfallows@bu.edu (K. Fallows), xiaohua.fang@lasp.colorado.edu (X. Fang), matt@ssl.berkeley.edu (M. Fillingim), caseyfly@bu.edu (C. Flynn), afogle@ssl.berkeley.edu (A. Fogle), christopher.fowler@lasp.colorado.edu (C. Fowler), jane.fox@wright.edu (J. Fox), fujimoto@stp.isas.jaxa.jp (M. Fujimoto), philippe.garnier@irap.omp.eu (P. Garnier), zachary.r.girazian@nasa.gov (Z. Girazian), hgr@lpl.arizona.edu (H. Groeller), jacob.r.gruesbeck@nasa.gov (J. Gruesbeck), ohamil@ku.edu (O. Hamil), kaha5350@colorado.edu (K.G. Hanley), hara@ssl.berkeley.edu (T. Hara), haraday@ssl.berkeley.edu (Y. Harada), jacob.hermann@lasp.colorado.edu (J. Hermann), mika.holmberg@irap.omp.eu (M. Holmberg), greg.holsclaw@lasp.colorado.edu (G. Holsclaw), sjh@ku.edu (S. Houston), inui@eps.s.u-tokyo.ac.jp (S. Inui), sonal.jain@lasp.colorado.edu (S. Jain), rebecca.jolitz@lasp.colorado.edu (R. Jolitz), akotova@irap.omp.eu (A. Kotova), tkuroda@pat.gp.tohoku.ac.jp (T. Kuroda), davin@ssl.berkeley.edu (D. Larson), Yuni.lee@nasa.gov (Y. Lee), clee@ssl.berkeley.edu (C. Lee), franck.lefevre@latmos.ipsl.fr (F. Lefevre), christy.lentz@lasp.colorado.edu (C. Lentz), rafael.a.lugo@nasa.gov (R. Lugo), yingjuan@ucla.edu (Y.-J. Ma), paul.r.mahaffy@nasa.gov (P. Mahaffy), melissamarquette@berkeley.edu (M.L. Marquette), ymatumot@astro.s.chiba-u.ac.jp (Y. Matsumoto), majdm@bu.edu (M. Mayyasi), cmazelle@irap.omp.eu (C. Mazelle), bill.mcclintock@lasp.colorado.edu (W. McClintock), mcfadden@ssl.berkeley.edu (J. McFadden), medvedev@mps.mpg.de (A. Medvedev), mendillo@bu.edu (M. Mendillo), milby@colorado.edu (Z. Milby), mitchell@ssl.berkeley.edu (D. Mitchell), ronan.modolo@latmos.ipsl.fr (R. Modolo), franck.montmessin@latmos.ipsl.fr (F. Montmessin), anagy@umich.edu (A. Nagy), rom@pat.gp.tohoku.ac.jp (H. Nakagawa), cnarvaez@bu.edu (C. Narvaez), kgolsen@umich.edu (K. Olsen), dpawlows@emich.edu (D. Pawlowski), william.peterson@lasp.colorado.edu (W. Peterson), rahmati@ssl.berkeley.edu (A. Rahmati), kjroeten@umich.edu (K. Roeten), norberto.romanelli@latmos.ipsl.fr (N. Romanelli), suranga-ruhunusiri@uiowa.edu (S. Ruhunusiri), ctrussell@igpp.ucla.edu (C. Russell), shotaro@eps.s.u-tokyo.ac.jp (S. Sakai), nick.schneider@lasp.colorado.edu (N. Schneider), k.seki@eps.s.u-tokyo.ac.jp (K. Seki), rshar@umich.edu (R. Sharrar), skylar.shaver@colorado.edu (S. Shaver), david.siskind@nrl.navy.mil (D.E. Siskind), marek.slipski@colorado.edu (M. Slipski), yasir.i.soobiah@nasa.gov (Y. Soobiah), msteckiewicz@irap.omp.eu (M. Steckiewicz), michael.stevens@nrl.navy.mil (M.H. Stevens), ian.stewart@lasp.colorado.edu (I. Stewart), arnaud.stiepen@ulg.ac.be (A. Stiepen), stone@lpl.arizona.edu (S. Stone), vtenishe@umich.edu (V. Tenishev), teradan@pat.gp.tohoku.ac.jp (N. Terada), kaneda@pat.gp.tohoku.ac.jp (K. Terada), ed.thiemann@lasp.colorado.edu (E. Thiemann), rhtolson@roadrunner.com (R. Tolson), gtoth@umich.edu (G. Toth), mvogt@bu.edu (M. Vogt), tristan.weber@colorado.edu (T. Weber), withers@bu.edu (P. Withers), shaosui.xu@ssl.berkeley.edu (S. Xu), eyigit@gmu.edu (E. Yiğit), rzurek@jpl.nasa.gov (R. Zurek).

https://doi.org/10.1016/j.icarus.2018.05.030

Available online 03 June 2018

[a] Laboratory for Atmospheric and Space Physics, University of Colorado, 3665 Discovery Dr., Boulder, CO 80303, United States
[b] IRAP, University of Toulouse, France
[c] Swedish Institute of Space Physics, Sweden
[d] NASA, Johnson Space Center, United States
[e] National Institute of Aerospace, U.S.
[f] NASA, Goddard Space Flight Center, United States
[g] Boston University, United States
[h] University of Michigan, United States
[i] LATMOS/CNRS, France
[j] CPI Inc., United States
[k] Kansas University, United States
[l] SSL, University of California at Berkeley, United States
[m] Princeton University, United States
[n] Virginia Tech, United States
[o] University of Arizona, United States
[p] Wright State University, United States
[q] JAXA, Japan
[r] University of Iowa, United States
[s] University of Tokyo, Japan
[t] Tohoku University, Japan
[u] Analytical Mechanics Associates, United States
[v] UCLA, United States
[w] Max Planck Inst. Solar System Research, Germany
[x] Eastern Michigan University, United States
[y] Naval Research Laboratory, United States
[z] University of Liege, Belgium
[A] George Mason University, United States
[B] NASA, Jet Propulsion Laboratory, United States
[C] University of New Brunswick, Canada

ARTICLE INFO

Keywords:
Mars
Atmosphere
Solar wind
Mars atmosphere
Mars climate
Magnetospheres

ABSTRACT

Observations of the Mars upper atmosphere made from the *Mars Atmosphere and Volatile Evolution* (*MAVEN*) spacecraft have been used to determine the loss rates of gas from the upper atmosphere to space for a complete Mars year (16 Nov 2014 – 3 Oct 2016). Loss rates for H and O are sufficient to remove ~2–3 kg/s to space. By itself, this loss would be significant over the history of the planet. In addition, loss rates would have been greater early in history due to the enhanced solar EUV and more-active Sun. Integrated loss, based on current processes whose escape rates in the past are adjusted according to expected solar evolution, would have been as much as 0.8 bar CO_2 or 23 m global equivalent layer of H_2O; these losses are likely to be lower limits due to the nature of the extrapolation of loss rates to the earliest times. Combined with the lack of surface or subsurface reservoirs for CO_2 that could hold remnants of an early, thick atmosphere, these results suggest that loss of gas to space has been the dominant process responsible for changing the climate of Mars from an early, warmer environment to the cold, dry one that we see today.

1. Introduction

There is compelling evidence that liquid water was abundant on early Mars, despite Mars being too cold today to sustain significant amounts of liquid water (e.g., Carr, 1986, 2007; Jakosky and Phillips, 2001). The most likely explanation, especially in the face of the Sun having been dimmer early in its history, is that early Mars had a more-effective greenhouse atmosphere (e.g., Pollack et al., 1987). Many of the key questions about Mars over the last three decades have centered on the nature and evolution of this early atmosphere. Measurements from spacecraft in orbit and on the surface indicate that there are insufficient carbonate deposits on the Mars surface and in the subsurface to hold enough CO_2 from this early, thicker atmosphere to provide significant greenhouse warming (Edwards and Ehlmann, 2015). In that context, the *Mars Atmosphere and Volatile Evolution* (*MAVEN*) mission was designed to explore the loss of gas to space at the present epoch in detail; the results on specific loss processes and their rates of loss would be used to infer the integrated loss to space through time and the degree to which loss to space can explain the changes inferred for the Martian climate (Jakosky et al., 2015a, b, c; Lillis et al., 2015). We report here the loss rates derived through a full Mars year of observations with *MAVEN*'s comprehensive instrumentation, and use these loss rates as the basis to extrapolate back in time to infer the time-integrated loss to space. These results will better constrain the role that loss of atmospheric gas to space has played in the changes in the Martian climate inferred from the surface morphology and mineralogy.

Loss to space can occur by a number of distinct processes that differ by constituent. We will focus on the most important processes for H and O escape, as they reflect loss of the climate-related gases CO_2 and H_2O: (i) Thermal (Jeans') escape of H, derived from photodissociation of H_2O and mediated by a chain of atmospheric chemistry and transport processes; (ii) acceleration of ions to escape velocity by electric fields; (iii) photochemical escape of hot O atoms (atoms with greater than thermal energy, derived from chemical reactions such as dissociative recombination in the ionosphere); and (iv) sputtering by pick-up ions, in which ions accelerated into the upper atmosphere by the solar-wind electric field can physically knock other atoms into space.

We discuss observations related to loss to space at the present epoch in section II, and integration to determine total amount of gas lost through time in section III.

2. Loss to space at the current epoch

2.1. MAVEN observations

The *MAVEN* spacecraft has been operating in its science mode since 15 November 2014, after a two-month on-orbit commissioning phase following orbit insertion on 21 September 2014. It completed a full

Mars year of science observations on 3 October 2016 and is on track to complete a second Mars year on 21 August 2018. The emphasis in this paper will be on the first Mars year of observations. Thus, our analyses include all Mars seasons, albeit during a limited portion of the solar cycle and with varying observing geometry. The spacecraft is in an elliptical orbit, with apoapsis near 6200 km altitude above the surface and periapsis typically near 150 km (with occasional "deep dip" excursions to ~125 km; periapsis actually tracks the atmospheric density rather than altitude, so these altitudes are representative; see Jakosky et al., 2015a). The orbit is inclined by ~74° relative to the Martian equator, driving precession in both the latitude and local solar time of periapsis. This precession allows the spacecraft to obtain coverage of all regions of near-Mars space, including the upstream solar wind, the bow shock, and magnetosheath and magnetic pile-up regions, the ionosphere, the wake downstream of the planet, and regions having different degrees of crustal remanent magnetism; unfortunately, not all regions can be observed at the same epoch from a single spacecraft. The deep dips provide coverage down to the lowermost part of the upper atmosphere, close to the transition to the homogenous lower atmosphere (Jakosky et al., 2015a).

MAVEN has nine science instruments that, collectively, observe directly or allow us to infer the properties of the Sun and solar wind that drive the system, the response of the upper atmospheric composition, structure, and dynamics, and the loss of neutrals and ions to space and the factors controlling them. We will not describe the instruments or measurements in detail here (see Jakosky et al., 2015a, c, and the detailed descriptions published in *Space Science Reviews*, vol. 195, numbers 1–4, 2015); the instruments are listed in Table 1. All nine *MAVEN* science instruments have operated well and have been collecting data as intended. Observations have been nearly continuous, with the exception of (typically) twice-weekly communications periods with Earth, a two-week communications blackout during solar conjunction (which did allow for limited observations), a small number of times with isolated instrument or spacecraft issues, and occasional communications relay passes with rovers on the surface.

2.2. Hydrogen loss

Hydrogen in the upper atmosphere is derived from the photodissociation of H_2O in the lower and middle atmosphere which converts some fraction of the H_2O into H_2 through odd-hydrogen reactions (McElroy and Donahue, 1972; Parkinson and Hunten, 1972; Yung et al., 1988). The H_2 is transported upward and dissociated in the upper atmosphere, producing atomic H. The H atom is light enough that, for typical thermospheric temperatures, those atoms at the high-energy tail of the Boltzmann distribution exceed Mars' escape velocity; those atoms near or above the nominal exobase will suffer few collisions and can escape to space. This thermal (or Jeans') escape is likely to be the primary mechanism by which H is lost to space. The combination of escaping atoms and atoms having sufficient energy to travel ballistically to high altitudes but not to escape creates an extended corona of H atoms surrounding Mars; this corona has been observed out past 10 R_M (e.g., Chaffin et al., 2015).

MAVEN can observe this extended H corona in at least four independent ways. First, the IUVS instrument observes solar Lyman-α photons scattered from the H atoms. It observes this both by looking at nadir (and seeing the entire column of gas within the corona) and by observing the extended corona by looking above the limb (McClintock et al., 2015). Second, SWIA and STATIC can observe H^+ ions created by ionization of exospheric H (Rahmati et al., 2017). Third, MAG can observe plasma waves generated by instabilities associated with H^+ ions (Romanelli et al., 2016).

Fourth, the SWIA instrument can observe the integrated column of H in the corona upstream of the bow shock (Halekas et al., 2015). Incoming solar-wind protons can undergo charge exchange with exospheric H, producing high-energy neutral H that can penetrate deeply into the atmosphere. When these penetrating protons become ionized again via electron stripping by atmospheric neutrals, they can be observed with SWIA. The number of observed H^+ ions depends on the density and speed of the solar wind (which are measured by SWIA) and the column abundance of Martian H in the corona outside of the bow shock, allowing the latter to be determined. The H abundance above the bow shock can be translated readily into the total column of H in the full corona and the seasonally dependent escape rate via Jeans' escape (Halekas, 2017). This approach is generally consistent with the ultraviolet remote-sensing measurements.

Fig. 1 shows the column abundance of H in the corona throughout the Mars year as observed from SWIA. There is an order-of-magnitude variation with season. This large-magnitude variation has been observed previously, both from *Mars Express* and from *Hubble Space Telescope* (Chaffin et al., 2014; Clarke et al., 2014), but the *MAVEN* observations follow the complete seasonal variation throughout a single Mars year.

The H loss rate is not measured directly, but can be calculated from the H abundance assuming or deriving a coronal temperature. For the range in observed column abundance and temperature, the loss rate varies between ~ 1–11 × 10^{26} H atoms s^{-1}. This is equivalent to a loss rate of ~ 160–1800 g of H per second (g H s^{-1}); assuming all of the H is coming from H_2O, this is the equivalent of removal of about 1400–16,000 g H_2O s^{-1}. At this rate, H from the entire column of atmospheric water at present (nominally, about 10 precipitable micrometers, or 10^{-3} g/cm^2) would be removed in about 3,000 – 30,000 years. Over 4.2 b.y., loss at this rate would remove a global layer of water between ~ 3.6–25 m thick (see Table 2). Although we have expressed this as loss of water, these measurements refer to the loss of H only; we expect O from water to be lost as well, but the O loss is complicated by the fact that it also can come from CO_2. Loss of O will be discussed below.

Although the seasonal variation could result from temperature variations within the exosphere itself and of a hot component of hydrogen (as proposed by Chaufray et al., 2007, and Bhattacharyya et al., 2015), a more-likely explanation stems from the seasonal variation in lower-atmospheric temperature (Chaffin et al., 2017). During the southern-summer season (L_s ~ 180–360°), increased atmospheric dust raises lower-atmospheric temperatures due to absorption of visible-wavelength sunlight. The higher temperatures allow water vapor to be carried up to higher altitudes without saturating the atmosphere. The production rates of H and H_2 are enhanced due to the decreased blocking of solar EUV photons by CO_2, and the H and H_2 resulting from photodissociation of the H_2O thereby start from a higher altitude and can be carried to the exobase more readily, resulting in an increased H abundance in the extended corona. Depending on the abundance and altitude of water transported upward, this effect could translate into a similar order-of-magnitude variation with season in the loss rates

Table 1
Science instruments on the MAVEN spacecraft.

Instrument Acronym	Name	Reference
NGIMS	Neutral Gas and Ion Mass Spectrometer	Mahaffy et al., 2015
IUVS	Imaging Ultraviolet Spectrograph	McClintock et al., 2015
EUVM	Extreme Ultraviolet Solar Monitor	Eparvier et al., 2015
STATIC	Suprathermal and Thermal Ion Composition	McFadden et al., 2015
SWIA	Solar Wind Ion Analyzer	Halekas et al., 2015
SWEA	Solar Wind Electron Analyzer	Mitchell et al., 2016
SEP	Solar Energetic Particle	Larson et al., 2015
LPW	Langmuir Probe and Waves	Andersson et al., 2015
MAG	Magnetometer	Connerney et al., 2015

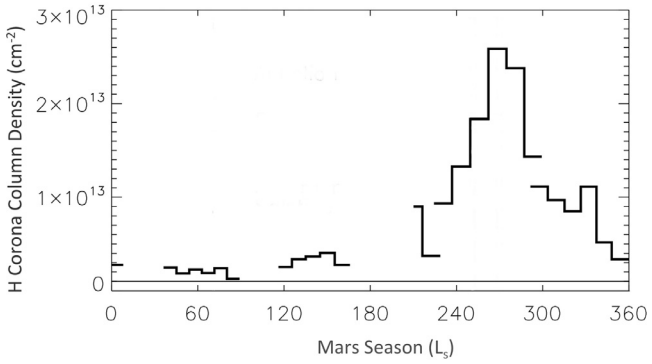

Fig. 1. H column density in the upstream direction, derived from SWIA measurements of penetrating H atoms. Jeans escape loss rates will have a comparable seasonal variation. From Halekas (2017).

(Chaffin et al., 2017; Halekas, 2017; Heavens et al., 2018).

If the loss rate of H is tied to the atmospheric dustiness, then the amount lost in a year is tied to the seasonal cycle of airborne dust. The seasonal dust behavior displays significant interannual variability (e.g., Zurek et al., 1992). Plus, the dust content and the water content of the atmosphere both are expected to vary with the obliquity of the planet, which varies on 10^5- and 10^6-year timescales (Jakosky et al., 1995). Thus, the loss rate definitely is not expected to have been constant with time and may vary significantly from year to year.

2.3. Oxygen ion loss

Ion loss occurs via the acceleration of ions in an electric field. The electric field can be generated around Mars by many different processes, including the moving magnetic field of the impinging solar wind (Luhmann and Kozyra, 1991), plasma pressure gradients in the ionosphere (Collinson et al., 2015), plasma flow shear near the strong crustal magnetic fields (Dubinin et al., 2008), movement of ions and electrons around the magnetic field in magnetic cusp regions (Ergun et al., 2016), or acceleration by magnetic tension forces associated with the draping of the external fields around the Mars "obstacle" to the solar wind, and with magnetic reconnection involving the crustal magnetic fields (e.g., Ma et al., 2017). These processes may start as deep down as the lower ionosphere (Ergun et al., 2016; Riousset et al., 2013, 2014).

MAVEN measures the composition and velocity of ions, using the STATIC instrument (McFadden et al., 2015). Although measurements can be made throughout the orbit, there is risk of counting ions twice depending on the exact path that they follow. To avoid this risk, Brain et al. (2015) tabulated the ion flow only when the spacecraft passes through an imaginary spherical shell surrounding Mars and having a radius centered on 1.35 R_M. The spacecraft passes through this shell twice per orbit, once inbound and once outbound, and the risk of double counting or incomplete counting then is minimal. Over the course of the mission, the spacecraft precession causes the measured locations to sweep through all latitudes smaller than the orbit inclination (between ± 74°) and all local times. The measurements have been sorted by the direction of the solar-wind convection electric field; this allows us to separate out acceleration directions relative to the orientation of the solar-wind magnetic field, and to identify different populations of escaping ions (Brain et al., 2015).

Fig. 2 shows the resulting map of escaping ions, as updated by Brain et al. (2017). The map utilizes so-called MSE coordinates (Mars–Sun-Electric field), defined such that the interplanetary magnetic field (IMF) lies in the x-y plane (with + y component) and the solar-wind motional electric field points in the + z direction. In the spherical representation of this figure, the IMF direction is in the equatorial plane (MSE latitude of 0°), and the motional electric field of the solar wind points toward the pole (MSE latitude of 90°, at the top of the figure). This map includes ions of all masses (with mass > 9 a.m.u.), with O^+ and O^{2+} being the dominant ions; it includes ion energies between 6 eV

Table 2
Summary of present-day loss rates and extrapolation through time. (References: L1992 = Luhmann et al. (1992); C2013 = Chassefiere et al. (2013); L2017 = Lillis et al. (2017).).

	H Jeans	O ion	O Dissoc Recomb	O sputtering	Total loss thru time
Present-day loss rate from MVN (s^{-1})	1.6-11 x 10^{26}	5 x 10^{24}	5 x 10^{25}	3 x 10^{24}	
4.2 b.y. at present rate, H_2O	3.6-25.2 m	0.2 m	2.2 m	0.14 m	
4.2 b.y. at present rate, CO_2		6 mbar	68 mbar	4 mbar	
CO_2 loss, extrap. from L1992		630 mbar	113 mbar	7 bar	7.7 bar
CO_2 loss, extrap. from C2013		525 mbar	227 mbar	42 mbar	0.79 bar
CO_2 loss, extrap. from L2017			460 mbar		0.46 bar
H_2O loss, extrap. from L1992		22.1 m	3.6 m	227 m	253 m
H_2O loss, extrap. from C2013		18.8 m	2.9 m	1.4 m	23 m
H_2O loss, extrap. from L2017			16 m		16 m

and 30 keV, with ~2 eV being the escape energy, so may be missing some low-energy escaping ions. The figure clearly shows that escape is minimized in the upstream direction (toward the Sun), enhanced in the tailward direction (away from the Sun), and also enhanced in a "polar plume" that accelerates ions from the upstream ionosphere in the direction of the electric field (Brain et al., 2015, 2017; Y. Dong et al., 2015).

As these measurements were taken throughout the entire first Mars year of *MAVEN* observations, they represent an average over one Mars year but also include variations due to the varying solar drivers, atmospheric boundary conditions, and factors that vary geographically such as crustal magnetic field strength and geometry. The integrated escape of ionized oxygen is obtained by summing up the exiting flux shown in the map, separately adding in the loss of both O^+ and O^{2+}. The net global loss rate for O atoms from both ions is 5×10^{24} s^{-1}, equivalent to a loss rate of ~130 g O s^{-1}. As a point of comparison, at this rate, the entire column of atmospheric O (present mainly as CO_2) would be removed in ~3 b.y. (Again, this is not to say that the loss rate was constant through time or that the O lost from the atmosphere is necessarily taken from CO_2; but these are useful numbers for comparison. These points will be addressed later.)

2.4. Photochemical loss

A variety of chemical processes result from the absorption of solar EUV photons in the Martian thermosphere (e.g., Schunk and Nagy, 2000). Many of these lead, either directly or indirectly (through subsequent reactions), to hot neutral atoms which populate the exosphere and can escape Mars' gravity if they have sufficient energy. The dominant source of hot and escaping O is the dissociative recombination of O_2^+ ions with ambient electrons. In 74% of the recombinations, the energy is sufficient both to break the O_2 bond and to give each of the resulting neutral O atoms an amount of energy (as kinetic energy) greater than the escape energy from Mars. When recombination occurs above the exobase, such that the upward-moving atom is not likely to be backscattered or slowed below escape energy by subsequent collisions, it will escape to space (e.g., Lillis et al., 2017; Fox and Hac, 2009; Lammer et al., 2008; Groller et al., 2014). (Dissociative recombination and photodissociative ionization can result in loss of N and C as well, but at much lower rates (Fox, 1993), and we will deal here only with O loss.)

MAVEN does not measure these escaping neutral O atoms directly. It does measure the upper-atmospheric ion composition and abundances and electron temperature and density, allowing the dissociative recombination rates to be calculated. It also measures the neutral composition and density, allowing the escape probability to be calculated. Altitude profiles of these two quantities (dissociative recombination rate and escape probability) allow the loss rate to be calculated (Lillis et al., 2017). The loss rate can be calculated for each orbit, with the resulting values being shown in Fig. 3. The loss rate varies dramatically through the mission due in part to the precession of the orbit: Measurements made near periapsis span a wide range of solar zenith angle and local time. Loss rates calculated for the night side of the planet, for example, are low due to the extremely tenuous ionosphere there (and the absence of the EUV photons that drive ionization). Loss rates are greater on the dayside, where there is a better-developed ionosphere. Loss flux also depends on EUV irradiance, which was significantly higher early in the mission. Fig. 3 shows the loss rates sorted by solar zenith angle and by EUV photoionization flux.

An independent approach to these calculations of neutral O escape utilizing mainly in-situ data is based on the remote sensing of the oxygen corona. IUVS observations, obtained from limb scans in lines including 130.4 and 135.6 nm, allow the construction of altitude profiles of the hot O (Deighan et al., 2015) which can then be fit with exospheric models to infer the escaping component (Lee et al., 2017).

A third approach toward constraining the neutral O exospheric densities, and thus the escaping component, is the observation of the most energetic escaping oxygen ions by the SEP detector on MAVEN (Rahmati et al., 2015, 2017). These ions, observed outside the bow shock, are produced from the exospheric O and "picked up" by the solar-wind convection electric field, which gives them their high (> several 10 s of keV) energies. Their observed fluxes can be interpreted in terms of the exospheric O reservoir from which they originate. This approach gives another way of deducing the exospheric O altitude profile and hence the exospheric escape rates.

The multiple approaches are generally consistent with each other. They yield loss estimates between about 3.5–7 $\times 10^{25}$ O s^{-1} (Lillis et al., 2017; Rahmati et al., 2017; Lee et al., 2015; Cravens et al., 2016), providing a measure of the uncertainty in the calculation based on the specific assumptions in the model. We' ll take the representative loss rate to be 5×10^{25} O s^{-1}, equivalent to loss of 1300 g O s^{-1}. At this rate, the O present as CO_2 in today's atmosphere would be lost in ~300 m.y.

2.5. Sputtering loss

The electric field generated by the solar wind accelerates ions from the ionosphere or corona. In one hemisphere (relative to the magnetic field), the accelerated ions will move away from the planet causing them to escape. In the other hemisphere, they can be accelerated into the planet, where they can collide with molecules in the upper atmosphere, a process termed "precipitation" (e.g., Luhmann and Kozyra, 1991; Luhmann et al., 1992). These precipitating O^+ ions will impact into the atmosphere at high velocities, up to twice the solar-wind velocity (or nearly 1000 km/s), and can transfer their momentum to atoms in the vicinity of the exobase via collisions and eject them to space. This sputtering process can be very effective in removing heavy neutral atoms (Luhmann et al., 1992), and is expected to have been the most significant mechanism for removing inert gases such as argon (Jakosky et al., 1994, 2017).

As mentioned earlier, *MAVEN* is not able to measure the escaping neutral atoms directly. However, it does measure the properties of the precipitating ions (those that collide with the upper atmosphere), including fluxes, composition, energy distribution, and direction (Leblanc et al., 2015), which are important inputs to the sputtering-loss calculations. Observations from near periapsis are used in order to determine the precipitating flux as close as possible to the exobase where the collisions occur. As a result, coverage of precipitating ions and calculations of sputtering closely follow the precession of the orbit; coverage is obtained at a wide variety of solar zenith angles (SZA), geographic locations, and local times, but is not complete. The sputtering loss rate is determined from these measurements based on the analytical formulation of Wang et al. (2015) that fits their multiple

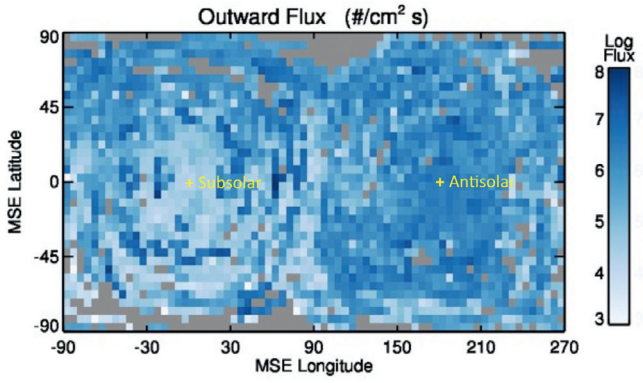

Fig. 2. Outward-moving flux of O ions (including both O^+ and O_2^+), shown as a function of MSE latitude and longitude (described in the text). From Brain et al. (2017).

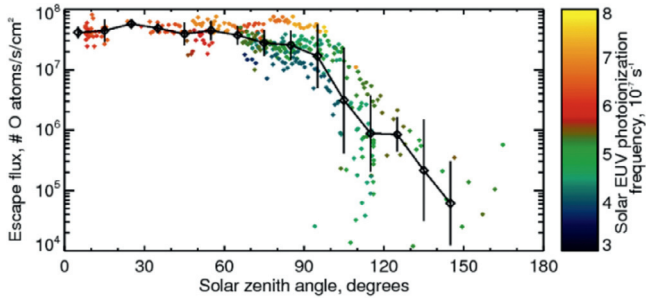

Fig. 3. O loss rates due to dissociative recombination, derived through the *MAVEN* mission over most of a Mars year (as described in the text). Data have been organized by solar zenith angle. Colors indicate EUV photoionization flux at the time of each measurement. After Lillis et al. (2017).

Monte-Carlo numerical simulations under various conditions (Leblanc et al., 2015).

For the year of observations of precipitating O^+ ions, the inferred average loss rate of neutral O due to sputtering is $\sim 3 \times 10^{24}$ O s^{-1}, equivalent to ~ 80 g O s^{-1}. At this loss rate, it would take more than 4 b.y. to remove the present-day atmospheric column of O.

2.6. Total loss rates at the present epoch

From these observations, we can derive the total loss rates over the year of observations made by *MAVEN*.

Jeans' escape of H is seasonally variable, between about 1–11 $\times 10^{26}$ H s^{-1}. These results are similar to observations made from *Mariner 6, 7*, and *9, Mars Express, Hubble Space Telescope*, and the *Rosetta* flyby of Mars (Fig. 4, and references contained therein), with the caveat that we do not fully understand the factors that drive either the seasonal variability or interannual variability. These estimates do not include possible loss of H via Jeans' escape of H_2. There has been only one observation of H_2 in the upper atmosphere (Krasnopolsky and Feldman, 2001), and model estimates of the loss rate as H_2 range from ~10% to twice the loss rate of H (e.g., Krasnopolsky, 2002; Yung et al., 1988).

The O ion loss rates derived from MAVEN are compared to earlier observational estimates of the loss rate from *Mars Express* in Fig. 5. These loss rates could be a lower limit if there are mechanisms for loss that have not been identified or observed. As an example, recent *MAVEN* observations have identified the loss of O^+ ions at energies just barely above the escape energy from Mars (Mitchell et al., 2017; Inui et al., 2018), but this loss has not yet been globally quantified. Similarly, the contributions to ionospheric plasma loss of bulk loss processes such as the breaking of unstable Kelvin-Helmholtz waves generated in the shear layer between the ionosphere and solar-wind plasmas (Ruhunusiri et al., 2017) are uncertain.

Summing up the O loss rates from all of the different processes, we estimate that the loss rate as observed by *MAVEN* is $\sim 6 \times 10^{25}$ O s^{-1}, as shown graphically in Fig. 6. The majority of today's identified O loss (either as neutrals or ions) is by photochemical loss (dissociative recombination).

H and O are being lost in ratio close to the value of 2:1 as would be appropriate for loss of H_2O, as postulated by McElroy (1972) and Liu and Donahue (1976). A 2:1 loss was suggested based on the feedback between build-up of either O or H in the atmosphere from photodissociation of water that results in an increase in the loss rate that pushed toward a net average loss of 2:1. Those calculations considered only photochemical loss of O and Jeans' escape of H; it's not clear how this feedback would operate when loss of O via ion processes or sputtering is included. Perhaps more importantly, there are time variations in the system that are shorter than the 10^3- to 10^5-year timescale on which O and H loss are expected to come to balance, potentially driving the system away from the steady-state condition required for 2:1 loss: (i) The factor-of-ten seasonal variation of the H loss rate suggests that there could be an interannual variation in loss rate that might be coupled to the year-to-year variation in the dust and dust-storm cycle; these variations are not understood on timescales from a decade to a century and longer (e.g., Zurek et al., 1992; Jakosky, 1995). (ii) There can be significant year-to-year variations in the amount of water vapor in the atmosphere (e.g., Jakosky and Barker, 1984) that would lead to significant interannual variations in the photodissociation and loss rates of H. (iii) Changes in the atmospheric water content are likely to occur on the timescale of the changes in the orbital elements (e.g., Jakosky et al., 1995) that could drive changes in loss rate that are recent enough to be reflected in today's escape rates. (iv) There could be other sinks for O and H (e.g., McElroy and Kong, 1976; Zahnle et al., 2008; Chassefiere et al., 2013; Lammer et al., 2003b); O could be oxidizing surface minerals, OH could be hydrating surface minerals, and loss of C could release O from CO_2 that would complicate the loss picture. Thus, it is premature to conclude that loss of H and O is occurring in the ratio of 2:1 for water.

We also can look at the total atmospheric loss at present. The loss rate of H to space today is at a rate between 160 – 1800 g H/s. Although the H almost certainly comes from H_2O, we cannot say definitively that this loss rate is equivalent to an H_2O loss rate of 1,400 – 16,000 g H_2O/s (obtained by taking the H loss rate and multiplying by the ratio of 18 a.m.u. for H_2O / 2 a.m.u. for 2 H), mainly because we have not fully identified the sink for O. The observed loss of O at present is occurring at a rate (summing up the loss from each identified process) of ~ 1500 g O/s. Thus, the total loss rate for H and O from the atmosphere to space at present is between ~2–3 kg/s.

In 4.2 b.y., loss of H at the observed rate would result in loss equivalent to loss of a global layer of H_2O between 3.6 – 25 m thick. At the present loss rate, the current column of atmospheric O would be lost in about 250 m.y.; equivalently, over 4.2 b.y. this would remove a total of ~78 mbar of CO_2. While significant, this amount in and of itself is not sufficient to explain loss of a presumed early, thick atmosphere. In addition, the O that is lost to space could come from either CO_2 or H_2O, both as a proximate source (e.g., for photochemical escape) and as the ultimate source (depending on removal of all atoms and to what sinks). If the escaping O ultimately comes from H_2O, it would be the equivalent of loss of a global layer of water about 2.5 m thick.

This is not a full picture of atmospheric loss at present, as there are other potentially significant effects that we have not yet accounted for. Examples includes the influence of the earlier presence and then loss of N via dissociative recombination (Fox, 1993), photochemical loss of C (Groller et al., 2014; Amerstorfer et al., 2017) or loss of deuterium (D) by Jeans' escape (Yung et al., 1988). In addition to the time dependences and potential forcing based on variations in the seasonal dust and water cycles (described above), we also have not incorporated the possible effects of atmospheric dynamical phenomena, such as gravity waves propagating into the upper atmosphere, on the escape process or rates (Yiğit et al., 2015). These and other additional factors

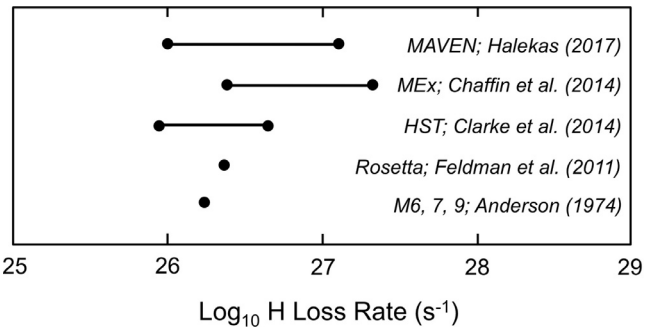

Fig. 4. H loss rate derived from observations made from different spacecraft.

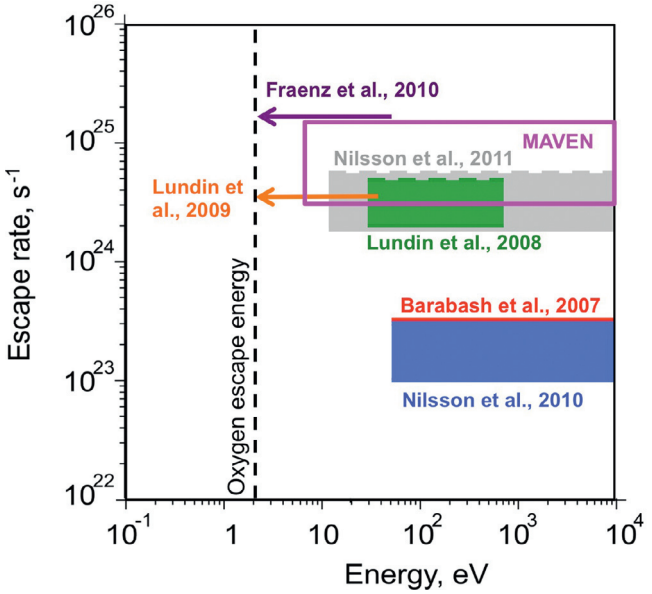

Fig. 5. Loss rate of O ions to space as derived from *MAVEN* observations and compared with *Mars Express* observations. Ranges show estimates of escape rates and the energy range over which measurements were made. O escape energy is shown.

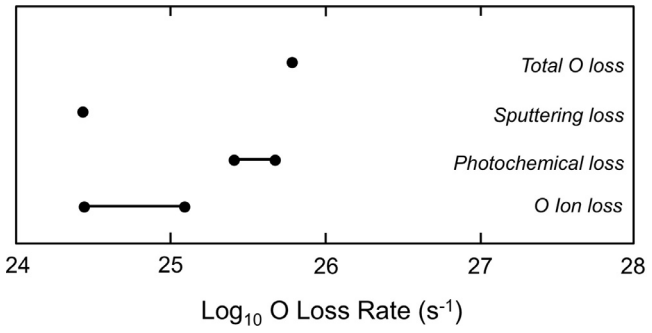

Fig. 6. O loss rate as determined from *MAVEN* observations for each of the loss processes examined.

eventually will be applied to our understanding of loss processes based on *MAVEN* results.

2.7. Solar-storm enhancement

There are several types of solar activity that can potentially affect the rates of loss of atmosphere to space, including flares in which the ionizing photon fluxes are greatly enhanced for short periods beyond the normal cycling of the Sun's EUV emissions, solar energetic particle (SEP) events that can enhance atmospheric ionization and potentially alter atmospheric chemistry, and coronal mass ejections (CMEs) that give rise to interplanetary plasma and field disturbances (termed interplanetary coronal mass ejections, or ICMEs) including shocks and enhanced solar-wind dynamic pressures and magnetic-field magnitudes. These solar events have the ability to enhance loss to space, as seen in both *Mars Express* and *MAVEN* observations (Jakosky et al., 2015b; Edberg et al., 2010). A preliminary analysis was made using *MAVEN* observations of the 8 March 2015 event, the largest ICME observed by *MAVEN* to date (Jakosky et al., 2015b). Enhancement in the apparent ion loss rate was seen at SZA ~ 40°, by a factor of ~10–20. However, no significant enhancement was seen in the downstream direction (SZA ~ 135°). This event exemplifies the difficulty of analyzing a single event from a single spacecraft – the orbital sampling and viewing geometry of *MAVEN* is limited during the several-day duration of a single event, and does not cover the full 4π solid angle surrounding Mars. To allow comparison with the "map" of escaping ions (Fig. 2), we used observations made only when *MAVEN* passed through the sphere surrounding Mars, as described earlier. This gives us measurements at only two locations in each orbit; they show a large spread in the outward-moving ion flux measurements, making definitive conclusions difficult. The approach used by Jakosky et al. (2015b) for getting the total escape was to calculate loss using global models of the solar-wind interaction during the ICME, with the models having been validated by detailed comparisons with the in-situ data from the individual orbits. This approach yielded an estimate of the enhancement in the total O loss rate (over all 4π solid angle) during that ICME by a factor of ~20 (Jakosky et al., 2015b; see also Curry et al., 2015, and C. Dong et al., 2015).

A second approach is to conduct a statistical analysis of all ICME events seen by *MAVEN*, as done by Curry et al. (2018). While a single event may not be definitive, the ensemble collection of all events covers a wider range of SZA and allows a statistical comparison that should be valid. In this approach, ICMEs were identified using pre-determined criteria related to the change in solar-wind velocity, density, and magnetic field when an ICME passed Mars. Fig. 7 shows the observed outward heavy-ion fluxes for the identified events, along with the average measurements of all observations for the year. By showing the events as a function of solar zenith angle, the effects of uncertainties in the magnetic-field orientation or other properties are minimized; note, however, that the map of escaping ions is not symmetric about the Mars-Sun line (i.e., at constant SZA), contributing to the large spread of loss rates at any given SZA.

The observations shown in Fig. 7 indicate that ICMEs result in a general decrease in the loss rate upstream, at low SZA, and an increase downstream, at higher SZA. As the plot shows the loss on a log scale, the up to 10x increase in flux at high SZA wins out over the similar-factor decrease at lower SZA. That is, there is a clear statistical enhancement in loss rate during ICME events (Curry et al., 2018). Integrating over SZA, the ensemble collection of these ICMEs produced a net factor-of-two enhancement in the loss rate. Because most of the ICMEs in this MAVEN sample are relatively small events, the effects of major events (not yet observed by *MAVEN*) are likely to be larger. We have not yet tried to integrate these into the *MAVEN* picture due to the lack of observations of extreme events; however, application of the

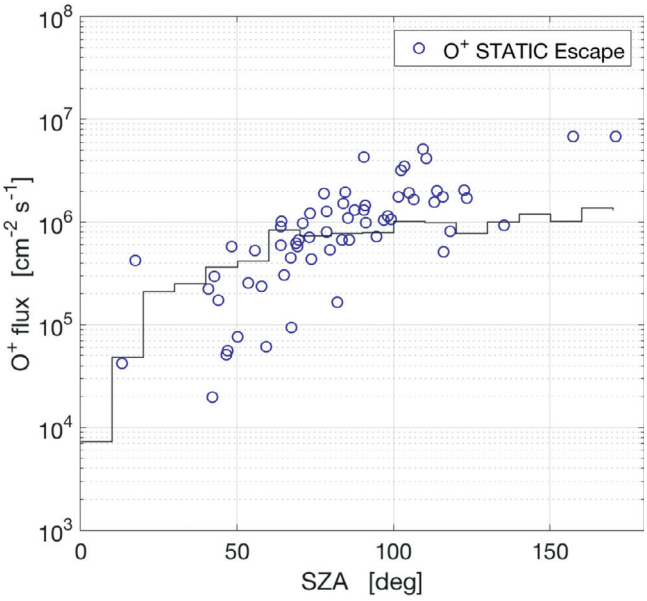

Fig. 7. Comparison of outward flux of O^+ ions as measured by STATIC during ICME events with average values over the full mission to date, shown as a function of solar zenith angle. From Curry et al. (2018).

MAVEN-validated solar-wind-interaction models to predicting the effects of large ICME events suggests that orders-of-magnitude enhancements in escape rates may occur (Luhmann et al., 2017).

3. Integrated loss through time

In this section, we first discuss the extrapolation back in time to the early history of Mars to obtain loss rates and the integrated loss based on our understanding gained from *MAVEN* observations. Second, we describe some of the uncertainties in the extrapolation, including lack of observations through the full solar cycle at present, changes in the solar outputs and activity cycle over time, changes in the obliquity of the Martian polar axis, the effects of changing the composition of the Martian atmosphere, and uncertainties in the modeled extrapolations.

Much of the extrapolation back in time is driven by the changing EUV and solar-wind properties of young Sun-like stars. These depend on the magnetic field of the star, which in turn depends on the rotation rate. The early Sun underwent a decline in the rotation rate, driven by the loss of angular momentum carried away by the early solar wind, and the slower rotation rate resulted in a weaker magnetic field (e.g., Newkirk, 1980; Ribas et al., 2005; Tu et al., 2015). Interestingly, the decline in the magnetically controlled solar EUV flux and solar-wind intensity early in history were accompanied by an increase in the total solar luminosity (mainly at visible wavelengths) as the Sun heated up due to the compression associated with the conversion of hydrogen to helium (Newkirk, 1980). This drove the seemingly contradictory behavior of Mars cooling off (apparently due to loss of a thick greenhouse atmosphere) at the same time that the Sun was heating up.

3.1. Extrapolation back in time

The major factors affecting atmospheric loss to space by present-day processes that were different early in Mars history were the EUV flux from the Sun, the nature of the solar wind, and solar activity. Models of the EUV flux and solar-wind conditions over time were first used to estimate the time-integrated escape via each process by Luhmann et al. (1992), with the extrapolations to early times indicating that loss rates could be orders of magnitude greater than they are today. These models have been updated since then as our understanding of the evolution of sun-like stars and of the escape processes themselves have improved. Here, we use the recent model of Chassefiere et al. (2013) to extrapolate back in time. Their model history of escape is shown in Fig. 8 for each of the major processes by which O can escape. In our extrapolation, we assume that the time variation of the loss rate is expressed by their functional form. We multiply their loss rates for each process by a constant factor in order to match the loss rate derived by *MAVEN* at the present. We use this as an interim approach until a detailed and fully self-consistent understanding of the loss processes at present can be developed and applied to past times.

Other models have been developed to estimate the integrated loss through time. In particular, Barabash et al. (2007) coupled measured rates of the loss of ions with energies greater than 30 eV with a 3D hybrid model of the Martian solar wind interaction developed by Modolo et al. (2005) to estimate the integrated loss of O^+ and O_2^+ to space. Boesswetter et al. (2010) carried out a similar analysis with a similar 3D hybrid model; Manning et al. (2011) convolved the results of several MHD models run for different solar wind input conditions with estimates of the time history of solar wind drivers to derive an estimate of atmospheric ion loss at Mars over time. Each of the above analyses focused on ion loss from Mars, based on the processes included in the model physics, neglecting loss of neutral particles.

Amerstorfer et al. (2017) examined the loss of hot O and C produced by dissociative recombination, using early EUV fluxes that would have enhanced loss; and Zhao and Tian (2015) examined the photochemical loss under high early EUV fluxes. These analyses focused on neutral loss, neglecting the loss of atmospheric ions. Lammer et al. (2003a, b) examined the various loss processes (both ion and neutral) for an assumed history of the EUV flux and solar wind in order to determine the integrated loss through time; these analyses included exchange with non-atmospheric reservoirs of volatiles as well as permanent loss of volatiles to the crust. Results summarized by Lammer et al. (2013) indicate a large variation in loss rates based on assumed solar and solar-wind properties and Mars regolith properties.

In choosing to compare our results with a small subset of models, rather than with each of the available models, we are taking the approach that the model results all are extremely uncertain in their detailed extrapolation back through time, but that they all result in significant enhancements in loss during the early epochs. Use of the Chassefiere et al. (2013) model provides a benchmark for demonstrating that integrated loss through time was substantial.

We use these loss rates to calculate the integrated loss to space from about 4.2 to 3.5 b.y.a. (billion years ago). This is the time period in which the geological observations provide evidence for a changing climate (e.g., Carr, 2007), and for which we wish to determine the role of loss to space. This time period is constrained on the early side by the time of onset of the geological record and the disappearance of the magnetic field. The earliest features in the geological record that show evidence for liquid water date to about 4.2 b.y.a. Loss that occurred prior to 4.2 b.y.a. predates the formation of these oldest features and would not have contributed to changes in the climate inferred from the geology. In addition, our expectation is that stripping of atmospheric gas by the solar wind is minimized by the presence of a magnetic field (e.g., Hutchins et al., 1997), although observations of escaping ions at Earth suggest that this may not be strictly correct (Strangeway et al., 2017). The shut-off of the Martian global magnetic field at about 4.1 b.y.a. (Lillis et al., 2008, 2013) thus may have allowed the turn-on of stripping of atmosphere to space. The rapid decline of the solar EUV and solar wind would have meant that the bulk of atmospheric loss would have occurred during the several-hundred-million-year period following loss of the magnetic field. In this sense, loss today is a small leak compared to the early loss, but serves to allow us to understand both how the specific physical loss processes operate and how respond to variation in the combined planetary conditions (such as seasonal cycles of dust and water) and solar and solar-wind drivers.

The Noachian era during which most of the water-related features occur ended at about 3.7 b.y.a. Water-related activity did continue into the Hesperian era, albeit at a declining rate, so we end our integration at 3.5 b.y.a.

The uncertainties in the extrapolation of today's loss rates back in time get very large prior to 3.5 b.y.a., due both to uncertainties in the

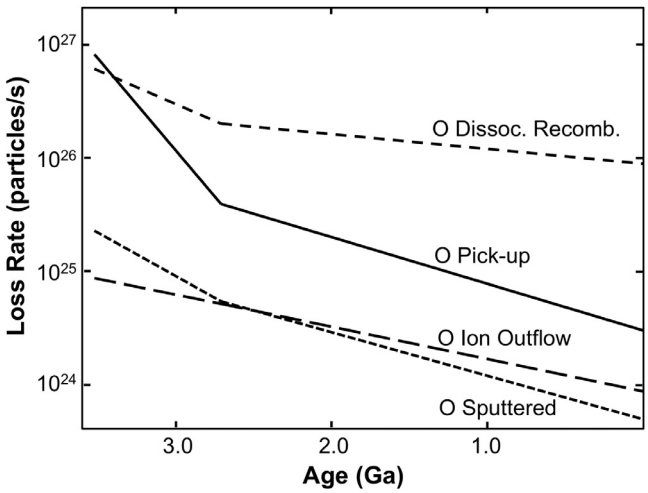

Fig. 8. Extrapolation of loss rates back through time for each relevant process. After Chassefiere et al. (2013).

solar properties and to increasing uncertainties due to expected non-linearities in extrapolating atmospheric composition and properties back farther in time. We take the approach of using the extrapolated loss rates at 3.5 b.y.a. and assuming that they also apply as a constant loss rate at earlier times. This likely underestimates the loss rates at the earliest times (perhaps by as much as an order of magnitude) and the integrated loss (by a factor of several). This conservative approach therefore gives us a lower limit on the extrapolated loss.

In addition to using the Chassefiere et al. (2013) model for loss due to dissociative recombination, we also extrapolated photochemical loss based on its observed EUV dependence (Lillis et al., 2017). This extrapolation has large uncertainties, due mainly to the scatter in the observations and the difficulty of fitting a unique exponential to a set of measurements and then extrapolating to EUV flux values well outside the range of values used in the fit (Lillis et al., 2017). In this extrapolation, we've also applied the loss rates appropriate for 3.5 b.y.a. to earlier times. The extrapolations of dissociative recombination may be problematic for the additional reason that expansion of the thermosphere during early epochs with high solar EUV flux may decrease the escape probability of atoms energized by dissociative recombination; this might limit the early loss rates to values below those based on the simple extrapolations (Zhao and Tian, 2015; Amerstorfer et al., 2017).

Integrated loss rates under these assumptions are given in Table 2; for comparison with earlier model estimates, we also include extrapolations based on the model of Luhmann et al. (1992). The integrated loss of O calculated as described above is equivalent to loss of greater than about 0.8 bar of CO_2, 23 m global equivalent layer of water, or some combination of the two depending on the source of the O atoms. These numbers can be compared with the integrated loss estimates assuming a constant loss rate through time based on present-day measurements of only ~78 mbar CO_2 and a few m of H_2O.

Extrapolation of the loss of H into the past is problematic. We already discussed the fact that simple exospheric theory based on solar EUV behavior alone does not explain the observed seasonal variation (Chaffin et al., 2017). We do not as yet fully understand what drives the seasonal behavior of the abundance of H in the corona. While the suggestion of dust raising atmospheric temperatures and allowing H_2O to rise higher into the atmosphere during southern summer is plausible, it has not been cleanly demonstrated from end to end (for example, by unambiguous detection of intermediate species in the chemical chain from H_2O to H, or by direct tracing of cause and effect due to an injection of atmospheric dust as described in a preliminary analysis by Heavens et al., 2018). Even if it is correct, we do not as yet understand the interannual variability in either the dust cycle or the lower-atmosphere water cycle. Thus, we cannot determine whether the Mars year observed by *MAVEN* is representative of the current epoch, or perhaps whether the extreme high or low values of H escape rate might be more representative of loss at the present.

Even if we understand the present-day H loss rate, it would be difficult to extrapolate to ancient times. On the one hand, loss could have been greater in ancient times than it is today based on the increased solar EUV flux (e.g., Ribas et al., 2005; Tu et al., 2015). The higher EUV flux would have increased the rate of photodissociation of water, and also would have provided additional heating of the upper atmosphere, both of which would increase the H escape rate. On the other hand, loss of H could have been lower in ancient times if, by having a more-Earth-like atmosphere, the Martian middle atmosphere had a more-efficient cold trap that kept the H_2O from getting as high in the atmosphere regardless of the dust behavior. This uncertainty even in the sign of the change in loss rate at earlier times makes extrapolation difficult. Integrated loss could have been as much as an order of magnitude greater than derived from the present loss rate. As we get a better understanding of the relative loss rates of D and H (utilizing the *MAVEN* IUVS observations of D; see Clarke et al., 2017), we hope to get a better understanding of the integrated loss of D through time; this would allow us to use the observed D/H as another way to infer the total amount of water lost through time.

An additional factor that has not been included in extrapolations to early times is the role of solar storms. The role of interplanetary coronal mass ejections (ICMEs) was discussed above, but not that of flares and SEPs – whose effects are still being analyzed. In addition, the non-uniform solar wind contains what are known as stream interactive regions (SIRs), where low and high speed wind from different solar source regions collide. Observations of sun-like stars suggest that, in addition to more flares and SEPs, these events occurred more often early in the Sun's history, providing a space environment of essentially continuous ICMEs and SIRs (Curry et al., 2018). As these events individually result in an enhancement in loss at the present, it seems likely that they may have had similar effects early in Mars' history. We do not have sufficient data yet to understand the cumulative contributions to atmospheric loss resulting from the largest events or how to extrapolate them back in time. However, because of their potential for enhancement of loss, the 0.8-bar loss described earlier again is likely to be a conservative lower limit on total loss, conceivably by orders of magnitude.

3.2. Factors affecting the extrapolation

We identify a number of factors that could affect our extrapolation into the past.

First is the fact that *MAVEN* has observed only a single Mars year, and that year was during the anomalous solar-cycle 24, with a delayed and low solar maximum (e.g., Gopalswamy et al., 2014). Thus, we have not yet seen the behavior at a more-typical solar maximum like that which occurred in cycles 20–22. *MAVEN* arrived at Mars after solar maximum and has not been in orbit long enough to observe at solar minimum, expected around 2020 (e.g., Hathaway, 2016). Again, this means that we do not know what behavior might be representative of loss as averaged over a full solar cycle, even a weak one.

Second, we have not explored the response of the loss rates to changes in the orbital elements of Mars. The axial obliquity varies from its present value, 25.2°, by large amounts; it can be as low as 0° or as high as 60°, and a long-term average may be closer to 40° (e.g., Laskar, 1989; Laskar and Robutel, 1993). Furthermore, the behavior is chaotic, in the sense that it cannot be calculated farther into the past than about 10 m.y.a. (million years ago) (Touma and Wisdom, 1993). Variations in obliquity can change the atmospheric pressure (by releasing CO_2 bound in the polar ice or adsorbed at high latitudes), the dust cycle (through changing of the seasonal winds or via a changed pressure), and the water cycle (through non-linear forcing by heating of the polar caps) (e.g., Kieffer and Zent, 1992). In addition, each of these seasonal cycles also will respond to changes in the orbital eccentricity and the argument of perihelion; together, these can make summer seasons more extreme in one hemisphere or the other, which also would change the forcing of both the seasonal water and dust cycles. The extent to which changing these factors can affect either the composition of the upper atmosphere or the escape rate is unknown.

Third, we have assumed in all of our extrapolations that the ancient atmosphere was identical in composition to the present-day atmosphere. An increase in total pressure at the surface would serve to raise the altitude of the exobase, changing the altitude at which the solar wind hits the atmosphere. By itself, this might not have a significant effect on loss rates. However, changes in the composition of the bulk atmosphere and upper atmosphere early in history would change the mixing ratios of different species at the exobase and thereby change both the relative and absolute escape rates. And, during this same time, outgassing of juvenile gases to the atmosphere would be expected to have occurred (e.g., Phillips et al., 2001) and would change the composition of the atmosphere. We expect that these changes could be quantitatively important but are not likely to change the qualitative behavior or conclusions.

Fourth, it's not clear what the early-epoch boundary conditions should be. Pepin (1994, and references therein) argued for an early

epoch of hydrodynamic outflow of H that could remove early atmospheric constituents very effectively by collisional-drag-induced escape of the heavy constituents. Although he suggested that this period ended around 4.4 b.y.a., the possible higher EUV fluxes described by Ribas et al. (2005) and Tu et al. (2015) may have pushed this to later times. The enhanced EUV may have heated the exosphere enough that C could have thermally escaped up until as late as 4.1 b.y.a. (Tian et al., 2009); this would have increased the early loss of CO_2 above that described here.

Fifth, the various models of solar interactions during the earliest epochs of Martian history show a wide range of rates of loss of gas to space. In part, this variation is due to uncertainties in the extrapolation of the EUV flux back in time, with the history of the Sun not necessarily being identical to the average behavior of Sun-like stars (Ribas et al., 2005; Tu et al., 2015). But in part it's also due to having to make assumptions or simplifications in the models to make them tractable. As an example, comparison of different models of the solar-wind interaction with Mars today produce a large range of possible behaviors and loss rates (Brain et al., 2010; Egan et al., 2018); extrapolation to different conditions outside of the range of observed interactions exacerbates those differences.

Despite these uncertainties in the extrapolation, it seems clear that loss to space was greater earlier in Martian history than it is today and that the integrated loss to space would have been substantial.

4. Conclusions

Even the present-day loss rates of Mars atmosphere constituents to space identified based on the *MAVEN* observations, by themselves and if constant through time, would result in a significant change in the abundance on Mars of both water and CO_2 through time. But these rates are not expected to have been constant with time and, given the processes at work, are expected to have been greater early in history. We have used the observed present-day loss rates to estimate the integrated escape over time by similar processes based on our understanding of the evolution of the Sun. Although this is a compelling argument, it is an argument based on plausibility and leaves us with some uncertainty.

For a direct indicator of total loss through time, we have used the *MAVEN* upper-atmospheric argon measurements. Jakosky et al. (2017) used the upper-atmosphere structure of the ratio of $^{38}Ar/^{36}Ar$ to derive the relationship between the isotopic fractionation in the bulk atmosphere and the fraction of gas that has been lost to space. Using the ratio as measured at the surface, this yielded a direct indicator of the fraction of gas lost; nearly 70% of the Ar that had ever been in the atmosphere must have been lost through time. Argon was lost by the sole process capable of removing a significant quantity of a noble gas, sputtering by pick-up ions. This result provides a direct indication that the bulk of the Martian atmosphere has been lost to space. In addition, the other isotopic ratios also indicate loss of a substantial fraction of the atmosphere to space. D/H and $^{15}N/^{14}N$ both show enrichment of the heavier isotope, indicative of loss of a major fraction of the gas to space (e.g., Owen et al., 1988; Villanueva et al., 2015; Fox, 1993; see also Kurokawa et al., 2018), providing a consistent view of atmospheric evolution.

In addition to loss by sputtering, CO_2 also would be subject to photochemical loss of both C and O. The timing of this loss as determined from the history of the Sun is consistent with that inferred from the geology of the surface. Combined with the lack of evidence for a substantial CO_2 reservoir on the surface or in the subsurface, we conclude that loss to space likely was able to quantitatively remove a postulated early, thick atmosphere. Loss to space appears to explain why the Mars atmosphere evolved from an early, warmer climate to the cold, dry climate that we see today.

Conflict of Interest

The authors have no competing financial interests.

Acknowledgments

The *MAVEN* mission was funded by NASA, initially through the Mars Scout program. We are indebted to the large number of people who are responsible for designing, building, testing, launching, operating, and communicating with the spacecraft and science instruments, as well as those responsible for the management, programmatic planning, budgeting, and funding of the project. Their efforts made this research possible. We thank two anonymous reviewers for very helpful comments.

References

Amerstorfer, U.V., Gröller, H., Lichtenegger, H., Lammer, H., Tian, F., Noack, L., Scherf, M., Johnstone, C., Tu, L., Guedel, M., 2017. Escape and evolution of Mars's CO_2 atmosphere: influence of suprathermal atoms. J. Geophys. Res. Planets 122, 1321–1337. http://dx.doi.org/10.1002/2016JE005175.

Andersson, L., Ergun, R.E., Delory, G.T., Eriksson, A., Westfall, J., Reed, H., McCauly, J., Summers, D., Meyers, D., 2015. The Langmuir probe and waves (LPW) instrument for MAVEN. Space Sci. Rev. http://dx.doi.org/10.1007/s11214-015-0194-3.

Barabash, S., Fedorov, A., Lundin, R., Sauvaud, J.-A., 2007. Martian atmospheric erosion rates. Science 315 (5811), 501–503. http://dx.doi.org/10.1126/science.1134358.

Bhattacharyya, D., Clarke, J.T., Bertaux, J.-L., Chaufray, J-Y., Mayyasi, M., 2015. A strong seasonal dependence in the Martian hydrogen exosphere. Geophys. Res. Lett. 42, 8678_8685.

Boesswetter, A., Lammer, H., Kulikov, Y., Motschmann, U., Simon, S., 2010. Non-thermal water loss of the early Mars: 3D multi-ion hybrid simulations. Planet. Space Sci. 58, 2031–2043.

Brain, D., Barabash, S., Boesswetter, A., Bougher, S., Brecht, S., Chanteur, G., Hurley, D., Dubinin, E., Fang, X., Fraenz, M., Halekas, J., Harnett, E., Holmstrom, M., Kallio, E., Lammer, H., Ledvina, S., Liemohn, M., Liu, K., Luhmann, J., Ma, Y., Modolo, R., Motschmann, U., Nagy, A., Nilsson, H., Shinagawa, H., Simon, S., Terada, N., 2010. A Comparison of Global Models for the Solar Wind Interaction with Mars. Icarus 206. http://dx.doi.org/10.1016/j.icarus.2009.06.030.

Brain, D.A., McFadden, J.P., Halekas, J.S., Connerney, J.E.P., Bougher, S.W., Curry, S., Dong, C.F., Dong, Y., Eparvier, F., Fang, X., Fortier, K., Hara, T., Harada, Y., Jakosky, B.M., Lillis, R.J., Livi, R., Luhmann, J.G., Ma, Y, Modolo, R., Seki, K., 2015. The spatial distribution of planetary ion fluxes near Mars observed by MAVEN. Geophys. Res. Lett. 42. http://dx.doi.org/10.1002/2015GL065293.

Brain, D., et al., 2017. MAVEN measurements of ion loss from Mars, abstract. In: Proceedings of the International Conference on Mars Aeronomy. Boulder.

Carr, M.H., 1986. Mars: A water-rich planet. Icarus 68, 187–216.

Carr, M.H., 2007. The Surface of Mars. Cambridge University Press, London.

Chaffin, M.S., Chaufray, J.-Y., Stewart, I., Montmessin, F., Schneider, N.M., Bertaux, J.-L., 2014. Unexpected variability of Martian hydrogen escape. Geophys. Res. Lett. 41 (2). http://dx.doi.org/10.1002/2013GL058578.

Chaffin, M.S., Chaufray, J.Y., Deighan, J., Schneider, N.M., McClintock, W.E., Stewart, A.I.F., Thiemann1, E., Clarke, J.T., Holsclaw, G.M., Jain, S.K., Crismani, M.M.J., Stiepen, A., Montmessin, F., Eparvier, F.G., Chamberlain, P.C., Jakosky, B.M., 2015. Three-dimensional structure in the Mars H corona revealed by IUVS on MAVEN. Geophys. Res. Lett. 42. http://dx.doi.org/10.1002/2015GL065287.

Chaffin, M.S., Deighan, J., Schneider, N.M., Stewart, A.I.F., 2017. Elevated atmospheric escape of atomic hydrogen from Mars induced by high-altitude water. Nature. http://dx.doi.org/10.1038/NGEO2887.

Chassefiere, E., Langlais, B., Quesnel, Y., Leblanc, F., 2013. The fate of early Mars' lost water: the role of serpentinization. J. Geophys. Res. 118, 1123–1134.

Chaufray, J.Y., Modolo, R., Leblanc, F., Chanteur, G., Johnson, R.E., Luhmann, J.G., 2007. Mars solar wind interaction: Formation of the Martian corona and atmospheric loss to space. J. Geophys. Res. 112. http://dx.doi.org/10.1029/2007JE002915.

Clarke, J.T., Bertaux, J.-L., Chaufray, J.-Y., Gladstone, G.R., Quemerais, E., Wilson, J.K., Bhattacharyya, D., 2014. A rapid decrease of the hydrogen corona of Mars. Geophys. Res. Lett. 41, 8013–8020. http://dx.doi.org/10.1002/ 2014GL061803.

Clarke, J.T., Mayyasi, M., Bhattacharyya, D., Chaurfary, J.Y., Bertaux, J.L., Chaffin, M., Schneider, N.M., Groller, H., Deighan, J., Jain, S., Villanueva, G.L., Jakosky, B., 2017. Estimating the hydrogen escape from Mars and understanding the D/H ratio, abstract. In: Proceedings of the International Conference on Mars Aeronomy. Boulder.

Collinson, G., Mitchell, D., Glocer, A., Grebowsky, J., Peterson, W.K., Connerney, J., Andersson, L., Espley, J., Mazelle, C., J.-A.Sauvaud, A.Fedorov, Ma, Y., Bougher, S., Lillis, R., Ergun, R., Jakosky, B.M., 2015. Electric Mars: The first direct measurement of an upper limit for the Martian "polar wind" electric potential. Geophys. Res. Lett. 42. http://dx.doi.org/10.1002/2015GL065084.

Connerney, J.E.P., Espley, J., Lawton, P., Murphy, S., Odom, J., Oliversen, R., Sheppard, D., 2015. The MAVEN magnetic field investigation. Space Sci. Rev. http://dx.doi.org/10.1007/s11214-015-0169-4.

Cravens, T.E., et al., 2016. Hot oxygen escape from Mars: Simple scaling with solar EUV irradiance. J. Geophys. Res. Space Phys. 122, 1102–1116. http://dx.doi.org/10.

1002/2016JA023461.
Curry, S.M., 2015. Response of Mars O+ pickup ions to the 8 March 2014 ICME: Inferences from MAVEN data-based models. Geophys. Res. Lett. 42, 9095–9102. http://dx.doi.org/10.1002/2015GL065304.
Curry, S.M., Luhmann, J.G., Dong, C.F., Hara, T., Gruesbeck, J., Halekas, J., Lee, C., Leblanc, F., Modolo, R., Ma, Y.J., Brain, D.A., McFadden, J., Espley, J., Connerney, J., Jakosky, B., 2018. MAVEN observations of atmospheric escape during space weather events in solar cycle 24. J. Geophys. Res in press.
Deighan, J., Chaffin, M.S., Chaufray, J.-Y., Stewart, A.I.F., Schneider, N.M., Jain, S.K., Stiepen, A., Crismani, M., McClintock, W.E., Clarke, J.T., Holsclaw, G.M., Montmessin, F., Eparvier, F.G., Thiemann, E.M.B., Chamberlin, P.C., Jakosky, B.M., 2015. MAVEN IUVS observation of the hot oxygen corona at Mars. Geophys. Res. Lett. 42. http://dx.doi.org/10.1002/2015GL065487.
Dong, C., et al., 2015a. Multifluid MHD study of the solar wind interaction with Mars' upper atmosphere during the 2015 March 8th ICME event. Geophys. Res. Lett. 42, 9103–9112. http://dx.doi.org/10.1002/2015/GL065944.
Dong, Y., Fang, X., Brain, D.A., P.McFadden, J., Halekas, J.S., Connerney, J.E., Curry, S.M., Harada, Y., Luhmann, J.G., Jakosky, B.M., 2015b. Strong plume fluxes at Mars observed by MAVEN: an important planetary ion escape channel. Geophys. Res. Lett. 42. http://dx.doi.org/10.1002/2015GL065346.
Dubinin, E., Chanteur, G., Fraenz, M., Woch, J., 2008. Field-aligned currents and parallel electric field potential drops at Mars. Scaling from the Earth' aurora. Planet. Space Sci. 56 (6), 868–872. http://dx.doi.org/10.1016/j.pss.2007.01.019.
Edberg, N.J.T., Nilsson, H., Williams, A.O., Lester, M., Milan, S.E., Cowley, S.W.H., Fränz, M., Barabash, S., Futaana, Y., 2010. Pumping out the atmosphere of Mars through solar wind pressure pulses. Geophys. Res. Lett. 37, L03107. http://dx.doi.org/10.1029/2009GL041814.
Edwards, C.S., Ehlmann, B.L., 2015. Carbon sequestration on Mars. Geology 43. http://dx.doi.org/10.1130/G36983.1.
Egan, H., Ma, Y., Dong, C., Modolo, R., Jarvinen, R., Bougher, S., Halekas, J., Brain, D., McFadden, J., Connerney, J., Mitchell, D., Jakosky, B., 2018. Comparison of global Martian plasma models in the context of MAVEN observations. Journal of Geophysical Research: Space Physics 123. http://dx.doi.org/10.1029/2017JA025068.
Eparvier, F.G., Chamberlin, P.C., Woods, T.N., Thiemann, E.M.B., 2015. The solar extreme ultraviolet monitor for MAVEN. Space Sci. Rev. 195. http://dx.doi.org/10.1007/s11214-015-0195-2.
Ergun, R.E., Andersson, L., Fowler, C., Woodson, A., Weber, T., Delory, G., Andrews, D., Eriksson, A., McEnulty, T., Morooka, M., Stewart, A.I.F., Mahaffy, P., Jakosky, B., 2016. Enhanced O_2^+ Loss at Mars due to an ambipolar electric field from electron heating. J. Geophys. Res. http://dx.doi.org/10.1002/2016JA022349. 7 May.
Fox, J.L., 1993. The production and escape of nitrogen atoms on Mars. J. Geophys. Res. 98, 3297–3310.
Fox, J.L., Hać, A.B., 2009. Photochemical escape of oxygen from Mars: a comparison of the exobase approximation to a Monte Carlo method. Icarus 204, 527–544. http://dx.doi.org/10.1016/j.icarus.2009.07.005.
Gopalswamy, N., Akiyama, S., Yashiro, S., Xie, H., Mäkelä, P., Michalek, G., 2014. Anomalous expansion of coronal mass ejections during solar cycle 24 and its space weather implications. Geophys. Res. Lett. 41, 2673–2680. http://dx.doi.org/10.1002/2014GL059858.
Groller, H., Lichtenegger, H., Lammer, H., Shematovich, V.I., 2014. Hot oxygen and carbon escape from the martian atmosphere. Planet. Space Sci. 98, 93–105.
Halekas, J.S., 2017. Seasonal variability of the hydrogen exosphere of Mars. J. Geophys. Res. Planets 122. http://dx.doi.org/10.1002/2017JE005306.
Halekas, J.S., Taylor, E.R., Dalton, G., Johnson, G., Curtis, D.W., McFadden, J.P., Mitchell, D.L., Lin, R.P., Jakosky, B.M., 2015. The solar wind Ion analyzer for MAVEN. Space Sci. Rev. 195, 125–151. http://dx.doi.org/10.1007/s11214-013-0029-z.
Hathaway, D., Solar cycle predictions, https://solarscience.msfc.nasa.gov/predict.shtml, 2016.
Heavens, N.G., Kleinbohl, A., Chaffin, M.S., Halekas, J.S., Kass, D.M., Hayne, P.O., McCleese, D.J., Piqueux, S., Shirley, J.H., Schofield, J.T., 2018. Hydrogen escape from mars enhanced by deep convection in dust storms. Nat. Astron. 2, 126–132. http://dx.doi.org/10.1038/s41550-017-0353-4.
Hutchins, K.S., Jakosky, B.M., Luhmann, J.G., 1997. Impact of a paleo-magnetic field on sputtering loss of Martian atmospheric argon and neon. J. Geophys. Res. 102, 9183–9189.
Inui, S., Seki, K., Namekawa, T., Sakai, S., Brain, D.A., Hara, T., McFadden, J.P., Halekas, J.S., Mitchell, D.L., Mazelle, C., DiBraccio, G.A., Jakosky, B.M., 2018. Cold dense ion outflow observed in the Martian-induced magnetotail by MAVEN. Geophys. Res. Lett. 45. https://doi.org/10.1029/2018GL077584.
Jakosky, B.M., 1995. Out on a limb: Martian atmospheric dust opacity during the past hundred years. Icarus 117, 352–357.
Jakosky, B.M., Barker, E.S., 1984. Comparison of ground-based and viking orbiter measurements of Martian water vapor: variability of the seasonal cycle. Icarus 57, 322–334.
Jakosky, B.M., Phillips, R.J., 2001. Mars' volatile and climate history. Nature 412, 237–244.
Jakosky, B.M., Pepin, R.O., Johnson, R.E., Fox, J.L., 1994. Mars atmospheric loss and isotopic fractionation by solar-wind-induced sputtering and photochemical escape. Icarus 111, 271–288.
Jakosky, B.M., Henderson, B.G., Mellon, M.T., 1995. Chaotic obliquity and the nature of the martian climate. J. Geophys. Res. 100, 1579–1584.
Jakosky, B.M., et al., 2015a. The MAVEN mission to Mars. Space Sci. Rev. http://dx.doi.org/10.1007/s11214-015-0139-x.
Jakosky, B.M., Grebowsky, J.M., Luhmann, J.G., Connerney, J., Eparvier, F., Ergun, R., Halekas, J., Larson, D., Mahaffy, P., McFadden, J., Mitchell, D.L., Schneider, N., Zurek, R., Bougher, S., Brain, D., Ma, Y.J., Mazelle, C., Andersson, L., Andrews, D., Baird, D., Baker, D., Bell, J.M., Benna, M., Chaffin, M., Chamberlin, P., Chaufray, Y.-Y., Clarke, J., Collinson, G., Combi, M., Crary, F., Cravens, T., Crismani, M., Curry, S., Curtis, D., Deighan, J., Delory, G., Dewey, R., DiBraccio, G., Dong, C., Dong, Y., Dunn, P., Elrod, M., England, S., Eriksson, A., Espley, J., Evans, S., Fang, X., Fillingim, M., Fortier, K., Fowler, C.M., Fox, J., Gröller, H., Guzewich, S., Hara, T., Harada, Y., Holsclaw, G., Jain, S.K., Jolitz, R., Leblanc, F., Lee, C.O., Lee, Y., Lefevre, F., Lillis, R., Livi, R., Lo, D., Mayyasi, M., McClintock, W., McEnulty, T., Modolo, R., Montmessin, F., Morooka, M., Nagy, A., Olsen, K., Peterson, W., Rahmati, A., Ruhunusiri, S., Russell, C.T., Sakai, S., Sauvaud, J.-A., Seki, K., Steckiewicz, M., Stevens, M., Stewart, A.I.F., Stiepen, A., Stone, S., Tenishev, V., Thiemann, E., Tolson, R., Toublanc, D., Vogt, M., Weber, T., Withers, P., Woods, T., Yelle, R., 2015b. MAVEN observations of the response of Mars to an interplanetary coronal mass ejection,. Science 350. http://dx.doi.org/10.1126/science.aad0210.
Jakosky, B.M., Grebowsky, J.M., Luhmann, J.G., Brain, D.A., 2015c. Initial results from the MAVEN mission to Mars. Geophys. Res. Lett. 42. http://dx.doi.org/10.1002/2015GL065271.
Jakosky, B.M., Slipski, M., Benna, M., Mahaffy, P., Elrod, M., Yelle, R., Stone, S., Alsaeed, N., 2017. Mars' atmospheric history derived from upper-atmosphere measurements of $^{38}Ar/^{36}Ar$. Science 355, 1408–1410.
Kieffer, H.H., Zent, A.P., 1992. Quasi-periodic climate change on Mars. In: Kieffer, H., Jakosky, B., Snyder, C., Matthews, M. (Eds.), Mars. University of Arizona Press, pp. 1180–1218.
Krasnopolsky, V.A., 2002. Mars' upper atmosphere and ionosphere at low, medium, and high solar activities: Implications for evolution of water. J. Geophys. Res. 107. http://dx.doi.org/10.1029/2001JE001809.
Krasnopolsky, V.A., Feldman, P.D., 2001. Detection of molecular hydrogen in the atmosphere of Mars. Science 294, 1914–1917.
Kurokawa, H., Kurosawa, K., Usui, T., 2018. A lower limit of atmospheric pressure on early Mars inferred from nitrogen and argon isotopic compositions. Icarus 299, 443–459.
Lammer, H., Kolb, C., Penz, T., Amerstorfer, U.V., Biernat, H.K., Bodiselitsch, B., 2003. Estimation of the past and present Martian water-ice reservoirs by isotopic constraints on exchange between the atmosphere and the surface. Int. J. Astrobiol. 2, 195–202.
Lammer, H., Lichtenegger, H.I.M., Kolb, C., Ribas, I., Guinan, E.F., Abart, R., Bauer, S.J., 2003b. Loss of water from Mars: Implications for the oxidation of the soil. Icarus 165, 9–25.
Lammer, H., Kasting, J.F., Chassefiere, E., Johnson, R.E., Kulikov, Y.N., Tian, F., 2008. Atmospheric escape and evolution of terrestrial planets and satellites. Space Sci. Rev. 139, 399–436.
Lammer, H., et al., 2013. Outgassing history and escape of the Martian atmosphere and water inventory. Space Sci. Rev. 174 113-154.
Larson, D., et al., 2015. The MAVEN solar energetic particle investigation. Space Sci. Rev. 195, 153–172. http://dx.doi.org/10.1007/s11214-015-0218-z.
Laskar, J., 1989. A numerical experiment on the chaotic behaviour of the solar system. Nature 338, 237–238.
Laskar, J., Robutel, P., 1993. The chaotic obliquity of the planets. Nature 361, 608–612.
Leblanc, F., Modolo, R., Curry, S., Luhmann, J., Lillis, R., Chaufray, J.Y., Hara, T., McFadden, J., Halekas, J., Eparvier, F., Larson, D., Connerney, J., Jakosky, B.M., 2015. Mars heavy ion precipitating flux as measured by Mars Atmosphere and Volatile EvolutioN. Geophys. Res. Lett. 42. http://dx.doi.org/10.1002/2015GL066170.
Lee, C.O., T.Hara, J.S.Halekas, Thiemann, E., Chamberlin, P., Eparvier, F., Lillis, R.J., Larson, D.E., Dunn, P.A., Espley, J.R., Gruesbeck, J., Curry, S.M., Luhmann, J.G., Jakosky, B.M., 2017. MAVEN observations of the solar cycle 24 space weather conditions at Mars. J. Geophys. Res. Space Phys. 122, 2768–2794. http://dx.doi.org/10.1002/2016JA023495.
Lillis, R.J., Frey, H.V., Manga, M., 2008a. Rapid decrease in Martian crustal magnetization in the Noachian era: Implications for the dynamo and climate of early Mars. Geophys. Res. Lett. 35, L14203. http://dx.doi.org/10.1029/2008GL034338.
Lillis, R.J., Robbins, S., Manga, M., Halekas, J.S., Frey, H.V., 2013. Time history of the Martian dynamo from crater magnetic field analysis. J. Geophys. Res. 118, 1488–1511. http://dx.doi.org/10.1002/jgre.20105.
Lillis, R.J., et al., 2015. Characterizing atmospheric escape from Mars today and through time with MAVEN. Space Sci. Rev. 195, 357–422.
Lillis, R.J., Deighan, J., Fox, J.L., Bougher, S.W., Lee, Y., Combi, M.R., Cravens, T.E., Rahmati, A., Mahaffy, P.R., Benna, M., Elrod, M.K., McFadden, J.P., Ergun, R.E., Andersson, L., Fowler, C.M., Jakosky, B.M., Thiemann, E., Eparvier, F., Halekas, J.S., Leblanc, F., Chaufray, J-Y., 2017. Photochemical escape of oxygen from Mars: First results from MAVEN in situ data. J. Geophys. Res. http://dx.doi.org/10.1002/2016JA023525.
Liu, S.C., Donahue, T.M., 1976. The regulation of hydrogen and oxygen escape from Mars. Icarus 28, 231–246.
Luhmann, J.G., Kozyra, J.U., 1991. Dayside pickup oxygen ion precipitation at Venus and Mars: Spatial distributions, energy deposition and consequences. J. Geophys. Res. 96, 5457–5467.
Luhmann, J.G., Johnson, R.E., Zhang, M.H.G., 1992. Evolutionary impact of sputtering of the martian atmosphere by O+ pickup ions. Geophys. Res. Lett. 19, 2151–2154.
Luhmann, J.G., Dong, C.F., Ma, Y.J., Curry, S.M., Xu, S., Lee, C.O., Hara, T., Halekas, J., Li, Y., Gruesbeck, J.R., Espley, J., Brain, D.A., Russell, C.T., Jakosky, B.M., 2017. Martian magnetic storms. J. Geophys. Res. Space Phys. 122, 6185–6209. http://dx.doi.org/10.1002/2016JA023513.
Ma, Y.J., Russell, C.T., Fang, X., Dong, C.F., Nagy, A.F., Toth, G., Halekas, J.S., Connerney, J.E.P., Espley, J.R., Mahaffy, P.R., Benna, M., McFadden, J., Mitchell,

D.L., Andersson, L., Jakosky, B.M., 2017. Variations of the Martian plasma environment during the ICME passage on 8 March 2015: a time-dependent MHD study. J. Geophys. Res. Space Phys. 122, 1714–1730. http://dx.doi.org/10.1002/2016JA023402.

Mahaffy, P.R., et al., 2015. The Neutral Gas and Ion Mass Spectrometer on the Mars Atmosphere and Volatile Evolution Mission. Space Sci. Rev. 195, 49–73.

McClintock, W.E., Schneider, N.M., Holsclaw, G.M., Clarke, J.T., Hoskins, A.C., Stewart, I., Montmessin, F., Yelle, R.V., Deighan, J., 2014. The Imaging Ultraviolet Spectrograph (IUVS) for the MAVEN mission. Space Sci. Rev. http://dx.doi.org/10.1007/s11214-014-0098-7.

McElroy, M.B., 1972. Mars: An evolving atmosphere. Science 175, 443–445.

McElroy, M.B., Donahue, T.M., 1972. Stability of the martian atmosphere. Science 177, 986–988.

McElroy, M.B., Kong, T.Y., 1976. Oxidation of the Martian surface: Constraints due to chemical processes in the atmosphere. Geophys. Res. Lett. 3, 569.

McFadden, J., et al., 2015. The MAVEN Suprathermal and thermal Ion Composition (STATIC) instrument. Space Sci. Rev. http://dx.doi.org/10.1007/s11214-015-0175-6.

Mitchell, D.L., Mazelle, C., Sauvaud, J.-A., Thocaven, J.-J., J.Rouzaud, A.Federov, Rouger, P., Toublanc, D., Taylor, E., Gordon, D., Robinson, M., Heavner, S., Turin, P., Diaz-Aguado, M., Curtis, D.W., Lin, R.P., Jakosky, B.M., 2016. The MAVEN Solar Wind Electron Analyzer. Space Sci. Rev. 200, 495–528. http://dx.doi.org/10.1007/s11214-015-0232-1.

Mitchell, D.L., Xu, S., Hara, T., Luhmann, J., Mazelle, C., McFadden, J., Andersson, L., DiBraccio, G., Connerney, J., 2017. Magnetic Topology and Ion Outflow in Mars' Magnetotail. In: Proceedings of the 14th Annual Meeting of the Asia Oceana Geosciences Society, Aug. 6-11Abstract PS03-D4-AM2-311-002.

Modolo, R., Chanteur, G.M., Dubinin, E., Matthews, A.P., 2005. Influence of the solar EUV flux on the Martian plasma environment. Ann. Geophy. 23, 1–12.

Newkirk Jr., G., 1980. Solar variability on time scales of 10^5 years to $10^{9.6}$ years. In: Pepin, R.O. (Ed.), Proceedings of the *Conference on Ancient Sun*. Houston. Lunar Planetary Institute, pp. 293–320.

Owen, T., Maillard, J.P., de Bergh, C., Lutz, B.L., 1767. Deuterium on Mars: The abundance of HDO and the value of D/H. Science 240 DOI: 10.1126/science.240.4860.1767, 1988.

Parkinson, T.D., Hunten, D.M., 1972. Spectroscopy and aeronomy of O2 on Mars. J. Atmos. Sci. 29, 1380–1390.

Pepin, R.O., 1994. Evolution of the Martian atmosphere. Icarus 111, 289–304.

Phillips, R.J., Zuber, M.T., Solomon, S.C., Golombek, M.P., Jakosky, B.M., Banerdt, W.B., Smith, D.E., Williams, R.M.E., Hynek, B.M., Aharonson, O., Hauck II, S.A., 2001. Ancient geodynamics and global-scale hydrology on Mars. Science 291, 2587–2591.

Pollack, J.B., Kasting, J.F., Richardson, S.M., Poliakoff, K., 1987. The case for a wet, warm climate on early Mars. Icarus 71, 203–224.

Rahmati, A., Larson, D.E., Cravens, T.E., Lillis, R.J., Dunn, P.A., Halekas, J.S., Connerney, J.E., Eparvier, F.G., Thiemann, E.M.B., Jakosky, B.M., 2015. MAVEN insights into oxygen pickup ions at Mars. Geophys. Res. Lett. 42. http://dx.doi.org/10.1002/2015GL065262.

Rahmati, A., et al., 2017. MAVEN measured oxygen and hydrogen pickup ions: Probing the Martian exosphere and neutral escape. J. Geophys. Res. Space Physics 122. http://dx.doi.org/10.1002/2016JA023371.

Ribas, I., Guinan, E.F., Gudel, M., Audard, M., 2005. Evolution of the solar activity over time and effects on planetary atmospheres. I. High-energy irradiances (1-1700 A). Astrophys. J. 622, 680–694.

Riousset, J.A., Paty, C.S., Lillis, R.J., Fillingim, M.O., England, S.L., Withers, P.G., Hale, J.P.M., 2013. Three-dimensional multifluid modeling of atmospheric electrodynamics in Mars' dynamo region. J. Geophys. Res. 118. http://dx.doi.org/10.1002/jgra.50328.

Riousset, J.A., Paty, C.S., Lillis, R.J., Fillingim, M.O., England, S.L., Withers, P.G., Hale, J.P.M., 2014. Electrodynamics of the Martian dynamo region near magnetic cusps and loops. Geophys. Res. Lett. 41, 1119–1125. http://dx.doi.org/10.1002/2013GL059130.

Romanelli, N., Mazelle, C., Chaufray, J.-Y., Meziane, K., Shan, L., Ruhunusiri, S., Connereny, J.E.P., Espley, J.R., Eparvier, F., Thiemann, E., Halekas, J.S., Mitchell, D.L., McFadden, J.P., Brain, D., Jakosky, B.M., 2016. Proton cyclotron waves occurrence rate upstream from Mars observed by MAVEN: associated variability of the Martian upper atmosphere. J. Geophys. Res. Space Physics 121 (11), 113–11128. http://dx.doi.org/10.1002/2016JA023270.

Ruhunusiri, S., et al., 2017. Characterization of turbulence in the Mars plasma environment with MAVEN observations. J. Geophys. Res. 122, 656–674. http://dx.doi.org/10.1002/2016JA023456.

Schunk, R.W., Nagy, A., 2000. Ionospheres: Physics, Plasma Physics, and Chemistry. Cambridge Univ. Press, New York.

Strangeway, R.J., Russell, C.T., Luhmann, J.G., Moore, T.E., Foster, J.C., Barabash, S.V., Nilsson, H., 2017. Does an intrinsic magnetic field inhibit or enhance planetary ionosphere outflow and loss. In: Abstract P11B-2506, Fall Meeting, Amer. Geophys. Union. New Orleans, Louisiana. pp. 11–15 Dec.

Tian, F., Kasting, J.F., Solomon, S.C., 2009. Thermal escape of carbon from the early Martian atmosphere. Geophys. Res. Lett. 36, L02205. http://dx.doi.org/10.1029/2008GL036513.

Touma, J., Wisdom, J., 1993. The chaotic obliquity of Mars. Science 259, 1294–1297.

Tu, L., Johnstone, C.P., Güdel, M., Lammer, H., 2015. The extreme ultraviolet and X-ray Sun in rime: High-energy evolutionary tracks of a solar-like star. Astron. Astrophys. 577. http://dx.doi.org/10.1051/0004-6361/201526146.

Villanueva, G.L., Mumma, M.J., Novak, R.E., Käufl, H.U., Hartogh, P., Encrenaz, T., Tokunaga, A., Khayat, A., Smith, M.D., 2015. Strong water isotopic anomalies in the martian atmosphere: Probing current and ancient reservoirs. Science 348 (6231). http://dx.doi.org/10.1126/science.aaa3630.

Wang, Y.-C., Luhmann, J.G., Fang, X., Leblanc, F., Johnson, R.E., Ma, Y., Ip, W.-H., 2015. Statistical studies on Mars atmospheric sputtering by precipitating pickup O^+: Preparation for the MAVEN mission. J. Geophys. Res. 120, 34–50. http://dx.doi.org/10.1002/2014JE004660.

Yiğit, E., England, S.L., Liu, G., Medvedev, A.S., Mahaffy, P.R., Kuroda, T., Jakosky, B.M., 2015. High-altitude gravity waves in the Martian thermosphere observed by MAVEN/NGIMS and modeled by a gravity wave scheme. Geophys. Res. Lett. 42, 8993–9000. http://dx.doi.org/10.1002/2015GL065307.

Yung, Y.L., Wen, J.-S., Pinto, J.P., Allen, M., Pierce, K.K., Paulsen, S., 1988. HDO in the martian atmosphere: Implications for the abundance of crustal water. Icarus 76, 146–159.

Zahnle, K., Haberle, R.M., Catling, D.C., Kasting, J.F., 2008. Photochemical instability of the ancient Martian atmosphere. J. Geophys. Res. 113. http://dx.doi.org/10.1029/2008JE003160.

Zhao, J., Tian, F., 2015. Photochemical escape of oxygen from early Mars. Icarus 250, 477–481.

Zurek, R.W., Barnes, J.R., Haberle, R.M., Pollack, J.B., Tillman, J.E., Leovy, C.B., 1992. Dynamics of the atmosphere of Mars. In: Kieffer, H.H., Jakosky, B.M., Snyder, C.W., Matthews, M.S. (Eds.), Mars. University of Arizona Press, Tucson, pp. 835–933.